EVS24
Stavanger, Norway, May 13-16, 2009

DC-DC converter for hybrid and all electric vehicles

P. James[1], A. Forsyth[2], G. Calderon-Lopez[2], V. Pickert [3]
[1]*Prodrive Ltd, UK*
[2]*University of Manchester, UK*
[3]*Newcastle University, UK*

Abstract

To realise the full potential of hybrid and all electric vehicle technologies, a step change is required in the performance of the DC-DC converter systems that connect the energy storage device and traction drive. This paper describes the work being done by a consortium to address these performance issues. It describes the requirements of such converters and details the electronics development of high efficiency converter techniques, thermal management design and health monitoring strategies and supports this work showing the results of simulation and prototype testing.

Keywords: DC-DC, efficiency, thermal management, health

1 Introduction

Power management in a hybrid or all electric vehicle is very important, and can directly determine whether the vehicle is 'good' or 'bad' not only in economy but also in drive-ability and ease of use. Power management is the way in which energy is moved to and from the energy storage device and the electric motor and includes the quantity of energy and the time over which it is done.

Energy storage or supply devices, e.g. super capacitors and fuel cells, vary their output voltage with load or state of charge and this creates major challenges for vehicle designers when integrating energy storage / supply devices with a traction drive. DC-DC converters can be used to interface the elements in the electric power train by boosting or chopping the voltage levels, but their use is limited due to the size, weight, efficiency and cost of current DC-DC converters.

This paper describes a new DC-DC converter currently being developed by a consortium of UK industrial and academic partners. The converter is being designed to operate within modern hybrid and electric vehicle systems and has low weight, small size, high efficiency, and is cost effective.

The advances reported in this paper include an efficient circuit topology, a high-performance, liquid-cooled heat sink, and real-time condition monitoring techniques for the power devices.

2 DC-DC converter

The bi-directional DC-DC converter is shown in Fig. 1 operating as a boost converter; power is drawn from the source v_{in} and delivered at a higher voltage to the load, represented by resistor R. By exchanging the positions of v_{in} and R, the circuit would operate as a buck converter and the load resistor voltage would be lower than v_{in}. For use as a supercapacitor interface, the supercapacitor would be connected on the low voltage side in parallel with C_{in}, whilst the high voltage side would be connected to the DC-link of the traction drive or the battery. For simplicity the operation of the circuit is described here as a boost converter. Hard and soft-switching versions of the circuit are described.

The converter consists of four IGBTs and anti-parallel diodes in an H-bridge configuration. The lower transistors Q_1 and Q_2 operate in an interleaved manner with equal duty-ratios of D whilst the complementary upper transistors operate in anti-phase with a small dead-time t_d. An interphase transformer (IPT) is used to combine the voltages at the mid-points of the two legs, points A and B, and the resultant voltage v_{com} has a value of $V_{AB}/2$, as sketched in Fig. 2 for the cases of D< 0.5 and D>0.5. Due to the interleaved operation of the transistors the AC component of v_{com} will be at twice the switching frequency, and as D tends to 0.5, v_{com} will become purely DC.

Assuming that the converter input current divides equally between the two IPT windings, the IPT core will operate with purely AC excitation, and apart from the magnetising energy the IPT is not required to store any energy. A low loss ferrite core may therefore be used. Due to the presence of the IPT the input inductor has a reduced AC excitation, especially for duty-ratio values in the region of 0.5, and may be designed using a high flux core.

In the hard switching converter the IPT is designed to have a high differential inductance. The sketched waveforms in Fig. 3 show the gate

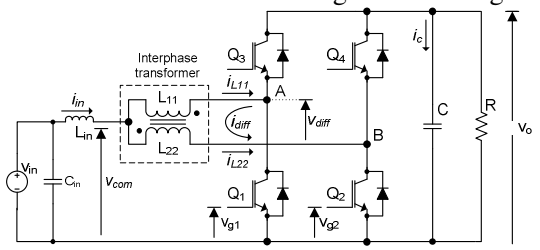

Figure 1: Hard-switched dual-interleaved boost converter with IPT.

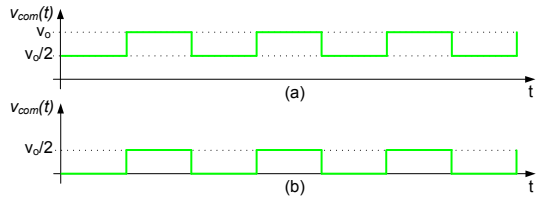

Figure 2: Ideal voltage at the mid-point of the IPT. (a) D< 0.5, (b) D> 0.5

driving signals of the first half-bridge, $v_{g1}(t)$ and $v_{g3}(t)$, the input current, $i_{in}(t)$, the current in the first winding of the IPT, $i_{L11}(t)$, and the collector-emitter voltage of Q_1, $v_{ce1}(t)$. In this case, the large differential inductance of the IPT between the nodes A and B produces a small differential current, i_{diff}. The current i_{L11} is therefore approximately equal to half of the input inductor current, crucially i_{L11} is always positive and therefore Q_3 does not conduct. Normal hard switching conditions result for Q_1 [1].

In the soft switching converter four additional snubber capacitors are added in parallel with the IGBTs and the IPT is designed with a much lower differential inductance. By reducing the differential inductance of the IPT, the differential current is increased so that the overall current in the IPT windings reverses transiently, as shown in Fig. 4. As a result, both IGBTs in each leg will conduct during the switching cycle and in each case, the anti-parallel diode conducts immediately before the IGBT itself [2]. By signalling the transistor on during the period of anti-parallel diode conduction, a smooth, virtually lossless transition occurs every switching period. Furthermore, the losses due to diode reverse-recovery are eliminated since the diodes are not subjected to a large reverse voltage immediately after conducting. The snubber capacitors limit the

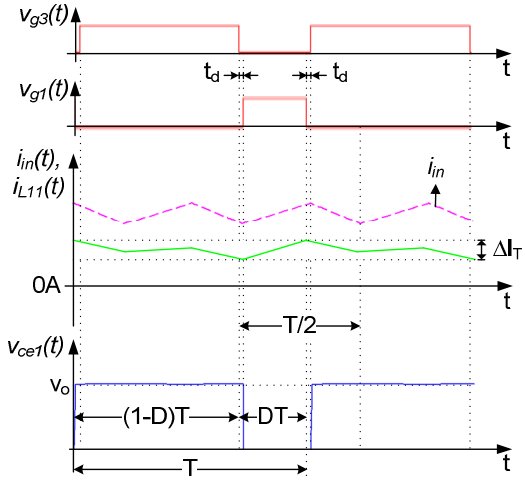

Figure 3: Idealised operating waveforms for the hard-switched converter with D< 0.5.

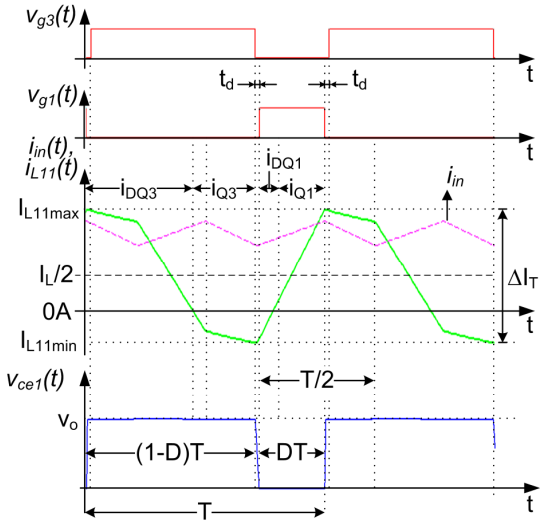

Figure 4: Idealised operating waveforms for the ZVS converter with D< 0.5.

turn-off losses in the transistors. For different duty ratio values, either equal to or greater than 0.5, and for reverse power flow, similar conditions occur.

2.1 Prototype converter

A ZVS converter prototype was designed to supply a 40 kW, 500 V load. The input inductor has a value of 50 µH and was wound on Metglas C-cores. The differential inductance of the IPT is 35 µH, and has a maximum peak-to-peak current value of 238 A for a duty ratio of 0.5.

To limit the core losses in the IPT, a ferrite core with a distributed gap structure was used to reduce the eddy current losses in the windings. The construction of the IPT is depicted in Fig. 5. Each winding limb was formed with a stack of 15 ring cores of 34 mm diameter with small spacers between the cores to create a distributed air gap. The top and bottom of the core were formed with ferrite 'I' pieces. The windings were made with 0.4 mm litz wire.

Semikron IGBT modules SKM400GB125D were used for the switching devices and the current sharing between the phases of the converter was achieved by using a peak current mode controller.

2.2 Experimental results

Fig. 6 shows the steady-state waveforms of the lower switch, Q_1, for the converter operating at 40 kW and v_o= 500 V. The switching frequency is 31 kHz, and the duty ratio is 0.4. Fig. 7 shows the detailed turn-on instant under the same conditions.

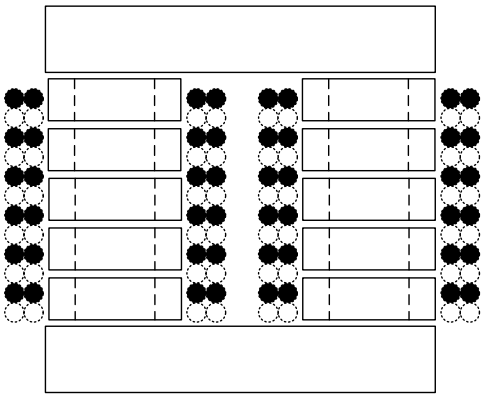

Figure 5: IPT core with distributed gap.

It can be seen that as soon as the voltage falls, the device has a negative current that is conducted by its anti-parallel diode. Clearly, the voltage is zero when the transistor starts conducting the positive current. Table 1 shows the estimated power losses in the components of the prototype. The efficiency was approximately 97%.

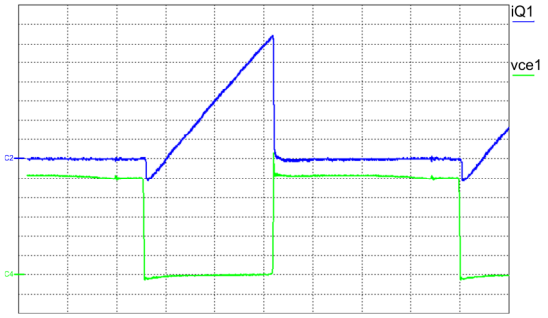

Figure 6: ZVS operation in IGBT Q_1: Ch2: i_{Q1}, 25 A/div, Ch4: v_{ce1}, 100 V/div, 5 µs/div. v_{in}= 300 V, v_o= 500 V, P_{in}= 40.8kW, P_o= 39.6 kW.

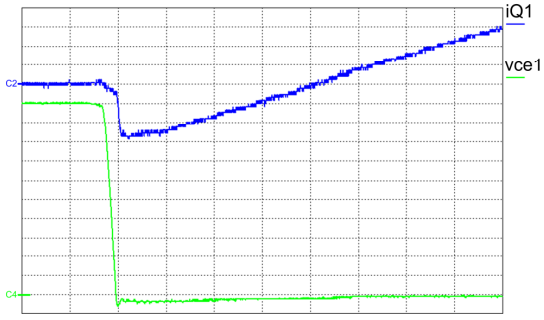

Figure 7: Detail of the turn-on transient of Q_1: Ch2: i_{Q1}, 10 A/div, Ch4: v_{ce1}, 50 V/div, 500 ns/div.

Table1: Estimated power losses for v_{in}= 300 V, 40 kW.

Losses in:	**Estimated (W)**
Semiconductors, conduction	300
Semiconductors, switching	500
IPT	200
Input inductor	50
Total	**1050**
Estimated efficiency	97 %

3 Thermal management

This section reviews the cooling concept applied to the converter. The two main components that generate significant heat are the power devices and the inductor/transformer. The power devices are dissipating up to 1.3kW where the inductor/transformer dissipates only 200W. Since the losses in the inductor/transformer are low, forced air cooling with a simple fan attached to the inductor and transformer is adequate. The cooling of the power devices is, however, more challenging due to the high power dissipation. In general heatsinks cover nearly a third of the volume and weight of power converters and therefore the heatsink design for the converter is of paramount importance in order to gain high power to volume/weight ratios.

It is well known that liquid cooling provides a much higher heat transfer coefficient then air cooling and therefore most power electronic systems in hybrid electric vehicles are liquid cooled.
Coolant flow can be through a simple folded tube arrangement bonded to a plate, or its equivalent by machined channels. Often these tubes or channels have a meander structure because there is a slight thermal advantage with re-entrant flow as a result of the bulk fluid mixing that takes place at the pipe bends. In designing a water-cooled heatsink the followings are some of the important design parameters:

1 Cost
2 Thermal performance
3 Water flow rater
4 Pressure drop
5 Mechanical strength
6 Corrosion & fouling
7 Manufacturability

Water flow rate and pressure drop influences the size of pumping and plumbing requirements and ultimately the cost and the physical volume of the coolant distribution system. Therefore in designing heatsinks, it is of great importance to minimize the water flow rates and the pressure drop, yet ensuring sufficient thermal performance [3].
At power densities above approximately 200W/cm^2 traditional cooling and power attachment methods become increasingly inadequate for presenting a low thermal resistance path. The project investigated in a technique to overcome these limitations by using pin-fin structures.
Pin-fin heatsinks refer to those designs in which the continuous straight fins of a conventional design are split into small discrete units [4]. This subdivision increases the surface that is available for heat transfer and causes formation of flow circulation regions near pin-fin surfaces. Both of these factors increase the heat transfer coefficient at the heatsink/fluid interface. Fig. 8 shows a pin-fin arrangement.

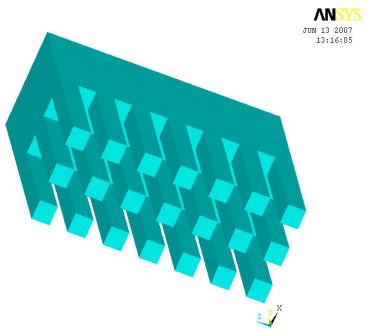

Figure 8: Pin fin structure

In order to achieve accurate coupled fluid flow and thermal simulation results, a CFD model of a millimetre scale pin-fin heatsink requires the use of a fine computational mesh, especially near the fin/fluid interface and across the flow channels. Fine meshing results in high demands on the computer resources and long solution times. To avoid difficulties, CFD heatsink analyses often use sub-models of the structure to evaluate an average heat transfer coefficient, and an incremental pressure drop.
Our own simulation work has shown that the most effective rectangular pin-fin to rear channel ratio is broadly 2:1. This ratio formed the basis for a comparison of the performance of different pin shapes with regard to heat transfer and incremental pressure drop.
For the elliptical and diamond fins, the cross-sectional aspect ratio is adjusted for equal area

and perimeter to the 2:1 ratio of the rectangular pin-fins. Circular fin diameter is adjusted for equal perimeter. Checks of the analyses were made with FE simulations of the sub-models to compare the temperature results obtained by applying average heat transfer coefficients against those from the CFD models.

The following pin-fin shapes have been investigated:

1 Rectangular
2 Circular
3 Diamond
4 Elliptical
5 Plain mm scale fins

The peak surface temperature and incremental pressure drop are compared in Table 2.

Table 2: Comparison of peak temperatures and pressure drops for various pin shapes

Type	Peak temperature (˚C)	Pressure drop (mBar)
Round	131	175
Elliptical	100	65
Diamond	137	121
Rectangular	132	95
Plain fin	140	70

Fig. 9 and Fig. 10 show two examples of the temperature profile of two different sub-models.

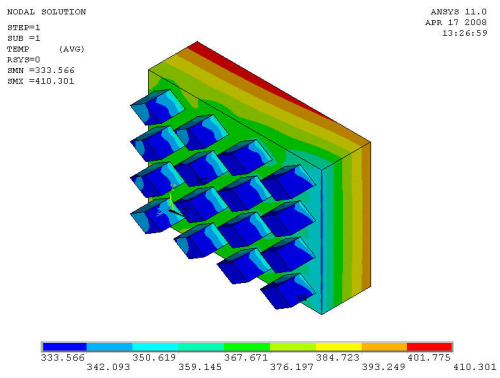

Figure 9: Diamond shaped fins

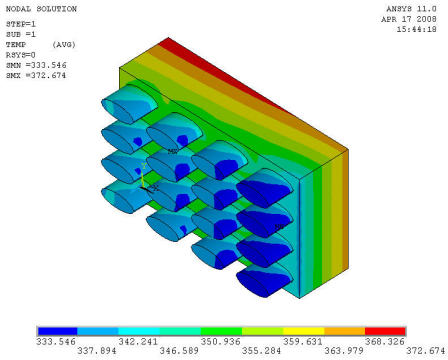

Figure 10: Elliptical shaped fins

As shown from Table 2 the elliptical shape fin structure provides an optimal solution in both low peak temperature and low pressure drop.

An aluminium heatsink was manufactured using the elliptical pin-fin structure with the 2:1 ratio and tested in the laboratory. The heatsink was connected to a heater/chiller that allows the water temperature to be set between +5^{o}C to +140^{o}C. Temperatures across the heatsink, pressure drop and flow-rate were measured. A resistor was placed on top of the heatsink to emulate the 1.3kW power dissipation. Fig. 11 shows the pressure drop measured over a 20min cycle. The average pressure is around 80mbar. The flow-rate is shown in fig. 12 with an average flow-rate speed of 5l/min. Finally the average temperature was measured to 56 ^{o}C (measured at six points distributed across the heatsink). The temperature fluctuation shown in fig. 13 is the result from the controller to keep the water temperature constant at 50^{o}C. The thermal mass of the process fluid causes a delay which results in the temperature fluctuation of +/-2 ^{o}C. The heatsink has the dimensions of 200mm*170mm*36mm.

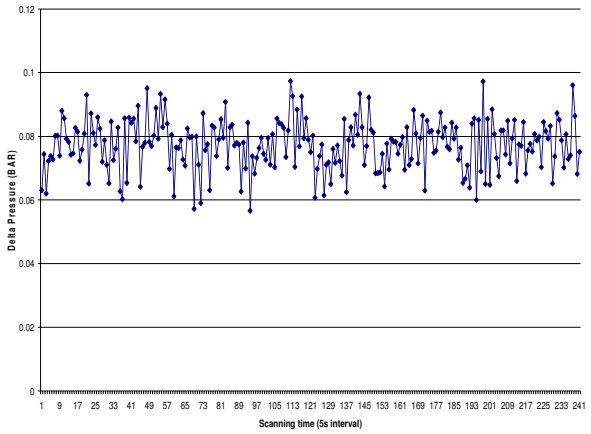

Figure 11: Pressure drop across the heatsink measured over a period of 20 minutes

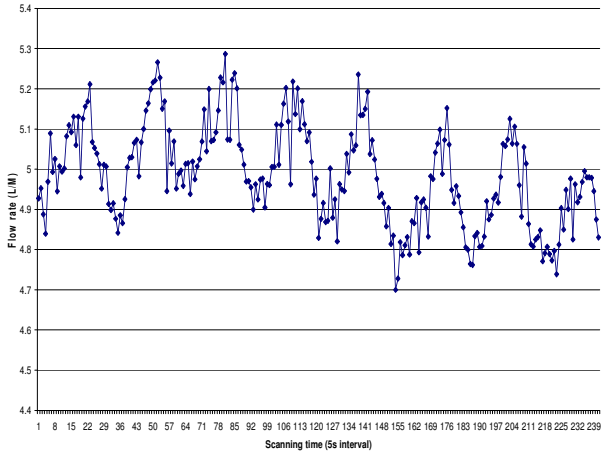

Figure 12: Flow-rate measured over a period of 20 minutes

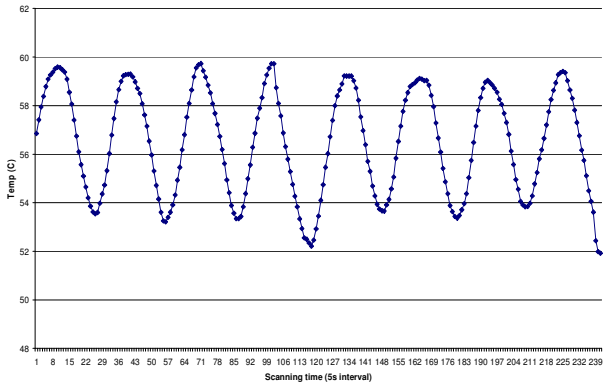

Figure 13: Average heatsink temperature measured over a period of 20 minutes

4 Prognostics

Another requirement of an automotive system is its ability to sense failure of part or all of the system and where possible predict this failure. Current power converters, including DC-DC converters, are usually tested to failure and the mean time to failure deduced. This value then becomes the normal operating life including some safety margin. For real world use this value is not practical as it is based on uniform operating parameters or unrealistic operating cycles. Real world operation, especially that of automotive systems is very random, in particular with regard to duty cycle and environment. It is therefore necessary to develop a health monitoring system that can predict the remaining life of the converter in real time. Research was carried out [5] looking at the failure modes and likelihood of failure of the main components of a DC-DC converter. The results can be seen in Table 3.

Table 3 – Failure cause and likelihood for DC-DC converter main components

Component	Likelihood of failure	Main cause of failure
Capacitor	72%	Increase in ESR
Semiconductor	24%	Thermal stress cracks
Inductor	3%	Shorting windings

These results show that the capacitors in a converter are the most likely cause of failure and there is much research done determining how they fail and how to predict their failure. The health monitoring system therefore uses capacitor ageing prediction as described in the referenced papers and the work described in this paper concentrates on predicting the failure of the semiconductor devices.

The failure mode of the semiconductor devices is due to their construction by materials with dissimilar coefficients of expansion [6]. During their normal operating life the devices heat up and cool down and this causes thermal stress in the device and eventually leads to failure. In order to develop a strategy for predicting failure an accelerated method to age and fail the device was required. In order to accelerate the test, the

flow of heat out of the IGBT module needs to be controlled. This is done by the use of Thermoelectric coolers based on the Peltier-Seebeck effect. Thermoelectric coolers are solid-state devices which move heat from one side of the cooler to another depending on the current flowing through the cooler. If the current is reversed the heat will flow in the opposite direction.

This controllable heat flow is used in the test rig to accelerate the temperature rise and fall of the IGBT module and thus reduce the time to failure of the module. The thermoelectric coolers are mounted between the IGBT module and heatsink. The base plate of the IGBT module is drilled to allow for a thermocouple to be placed as close as possible to the semiconductor junction and heatsink compound is used between all contact surfaces to ensure best thermal conductivity. The test cycle is as follows: The IGBT gate is switched on and the thermoelectric coolers activated so as to take heat out of the heatsink and into the base plate of the IGBT module. When the junction temperature reaches the maximum for the device the IGBT is switched off and the polarity of the current to the thermoelectric coolers reversed. When the junction temperature reaches the minimum a cycle counter is incremented and the cycle repeats. During the heating or ON cycle the Vce of the IGBT is also monitored and if this value increases by 20% from the original value the IGBT is regarded as having failed and the test stops.

In order to validate the accelerated lifeing methodology a Fuji Electric IGBT was used. This IGBT was rated at 600V and 50A, therefore the load that the IGBT was driving during the on phase of the experiment was set to 50A.

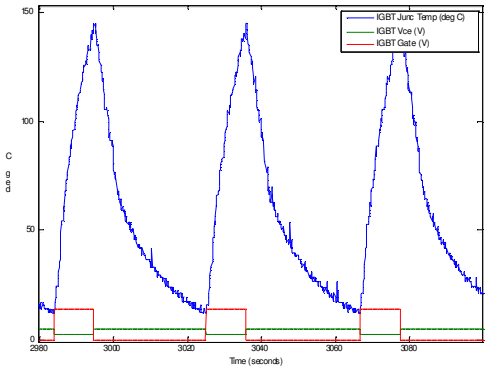

Figure 14: IGBT Junction temperature, gate voltage and Vce

Figure 14 shows the junction temperature for three cycles along with the gate pulse and measured Vce. Initial testing of the IGBT modules uses a minimum temperature of 10ºC and a maximum temperature of 150ºC, which is the maximum specified in the manufacturer's data sheet. The test rig is achieving a temperature rise of 140ºC in about 12 seconds giving a temperature rise rate of 12ºC per second. The test rig was able to fail an IGBT module in 1427 cycles. The point of failure can be seen in Figures 15 and 16.

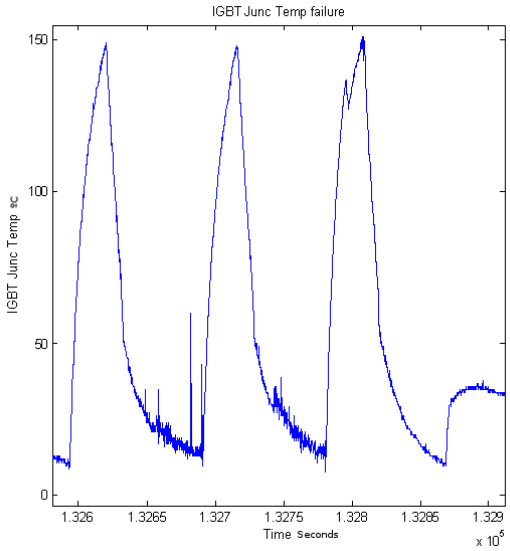

Figure 15: IGBT Junction temperature at point of failure

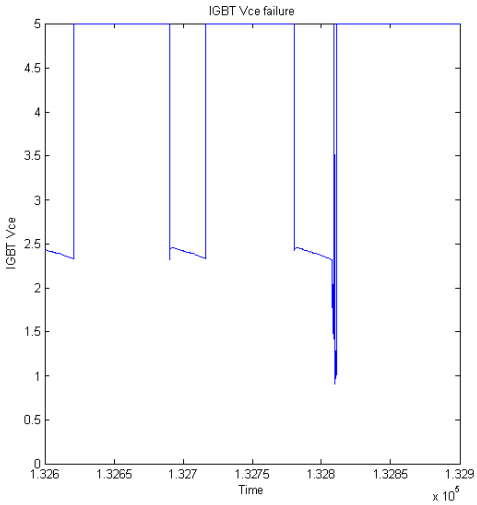

Figure 16: IGBT Vce at point of failure

This failure time is around 20 times faster than test methods which don't use thermoelectric coolers and the number of cycles to failure is consistent with results from these other test

methods.
This life data can then be used by prognostic algorithms to predict the failure of the IGBT modules in real time.

5 Conclusion

In order for a DC-DC converter to be used on an automotive vehicle certain design criteria need to be fulfilled. This paper has described three areas of efficiency, thermal management and prognostics where development was required to meet the requirements of the automotive industry.
The dual interleaved topology for the DC-DC converter using and IPT allows high conversion efficiencies (97%) to be achieved in a 40 kW prototype whilst minimising the components sizes. Furthermore, soft-switching may be easily incorporated to reduce switching losses. These advances allow the converter to be considered for vehicle systems where high efficiency is critical for example all-electric vehicles.
The efficient thermal management of the power devices has resulted in a compact converter which is straight forward to package in a vehicle design.
The prognostics and health monitoring has enabled the DC-DC converter to provide similar functionality to that already available on IC engines and dependability that is essential to vehicle manufacturers.

References

[1] G. Calderon-Lopez, A. J. Forsyth, and D. R. Nuttall, *Design and Performance Evaluation of a 10-kW Interleaved Boost Converter for a Fuel Cell Electric Vehicle*, CES/IEEE International Power Electronics and Motion Control Conference, China,vol.2, pp. 1328-1332, 2006.

[2] G. Calderon-Lopez and A. J. Forsyth, *High-Power Dual-Interleaved ZVS Boost Converter with Interphase Transformer for Electric Vehicles,* IEEE Applied Power Electronics Conference and Exposition, APEC 2009, Washington DC, USA, 2009.

[3] Churchill, S.W., *"Comprehensive Correlating Equations for Heat, Mass and Momentum Transfer in Fully Developed Flow in Smooth Tubes"*, Ind. Eng. Chem. Fundam., Vol. 16, No. 1, pp.109-l 16, 1977.

[4] Xiaoling Y. et al., *"Development of a plate-pin fin heat sink and its performance comparisons with a plate fin heat sink"*, Applied Thermal Engineering Journal, Vol., 25, pp. 173–182, Elsevier, 2005.

[5] Military Handbook 217F, *Reliability Prediction of Electronic Equipment*, 1995.

[6] Ciappa, M and Fichtner, W, *Lifetime Prediction of IGBT Modules for Traction Applications*, IEEE 38th Annual International Reliability Physics symposium, 2000.

Acknowledgements

Consortium members: Prodrive Ltd, HILTech Developments, University of Manchester, Newcastle University, International Transformers, LDV Ltd, Sloan Electronics Ltd, EVO Electric Ltd

Len Pritchard – Newcastle University

The authors would like to thank the Technology Strategy Board, UK for their support of this research.

Authors

Pete James was awarded his bachelors degree in Electronic Engineering from Lancaster University. Since graduating he has worked for several companies in various industries including designing uninterruptible power supplies and automotive diagnostic systems. He has spent the last 12 years working for Prodrive and is currently a Technical Specialist working on high power electronics and studying for a PhD in prognostics for power converters.

Andrew Forsyth received the B.Sc.(Eng) degree from Imperial College, London, U.K., in 1981 and the Ph.D. degree from the University of Cambridge, Cambridge, U.K., in 1987. Since 2004 he has been Professor of Power Electronics at the University of Manchester, Manchester U.K. His research interests include high-frequency converters, high-power-factor rectifiers, modelling and control of autonomous power systems, aerospace and electric vehicle applications.

Gerardo Calderon-Lopez received the degree of Communications and Electronic Engineering from the National Polytechnic Institute (IPN) of Mexico in 1999, the Masters degree in Power Electronics and Drives from The Universities of Birmingham and Nottingham, U.K. in 2001, and recently the Ph.D. degree from The University of Manchester, U.K. His research interests include the design, modelling and control of hard and soft-switched DC/DC converters for electric vehicles.

Volker Pickert received his Dipl.-Ing. in Electrical and Electronic Engineering from the RWTH Aachen, Germany and the University of Cambridge, UK in 1994. He received his PhD from Newcastle University in 1997. In 1998 he started at Semikron International as application engineer and moved later to Volkswagen where he became group leader for electric drives for electric-, hybrid- and fuel cell vehicles. Since October 2003 he is a Senior Lecturer at Newcastle University. His research interests are power electronics for automotive applications, thermal management, fault tolerant converters and nonlinear controllers.